Electronic Supplementary Information (ESI)

Understanding the bactericidal mechanism of $Cu(OH)_2$ nanorods in water through Mg-substitution: high production of toxic hydroxyl radicals by non-soluble particles

*Batiste CLAVIER [1], Téo BAPTISTE [1], Antonii ZHADAN [1], Amandine GUIET [1], Fabien BOUCHER [2], Vlasta BREZOVÁ [3], Christine ROQUES [4,5] and Gwenaël CORBEL [1]**

[1] Institut des Molécules et Matériaux du Mans (IMMM), UMR-6283 CNRS, Le Mans Université, Avenue Olivier Messiaen, 72085 Le Mans Cedex 9, France
[2] Institut Universitaire de Technologie du Mans, Le Mans Université, Avenue Olivier Messiaen, 72085 Le Mans Cedex 9, France
[3] Institute of Physical Chemistry and Chemical Physics, Faculty of Chemical and Food Technology, Slovak University of Technology, Radlinského 9, SK-812 37 Bratislava, Slovakia
[4] Laboratoire de Génie Chimique, UMR-5503 CNRS, Faculté de Pharmacie, Université Paul Sabatier - Toulouse III, 35, chemin des maraîchers, 31 062 Toulouse Cedex 4, France
[5] Centre Hospitalier Universitaire (CHU) de Toulouse, Institut Fédératif de Biologie (IFB), Laboratoire de Bactériologie et Hygiène, 330 Avenue de Grande Bretagne, 31059 Toulouse Cedex 9, France

* To whom correspondence should be addressed
Institut des Molécules et Matériaux du Mans (IMMM)
UMR-6283 CNRS, Le Mans Université
Avenue Olivier Messiaen, 72085 Le Mans Cedex 9, France
Tel.: +33 (0)2 43 83 26 48 FAX : +33 (0)2 43 83 35 06
E-mail: gwenael.corbel@univ-lemans.fr
ORCID: 0000-0003-2605-7702

S1. Experimental details

S1.1 Optical absorption spectroscopy.

UV-Visible-Near-IR optical absorption spectra were measured on solutions in the range 400-1400 nm with a Shimadzu UV-2600 spectrophotometer. The spectral resolution is 1 nm in the range 400-1400 nm.

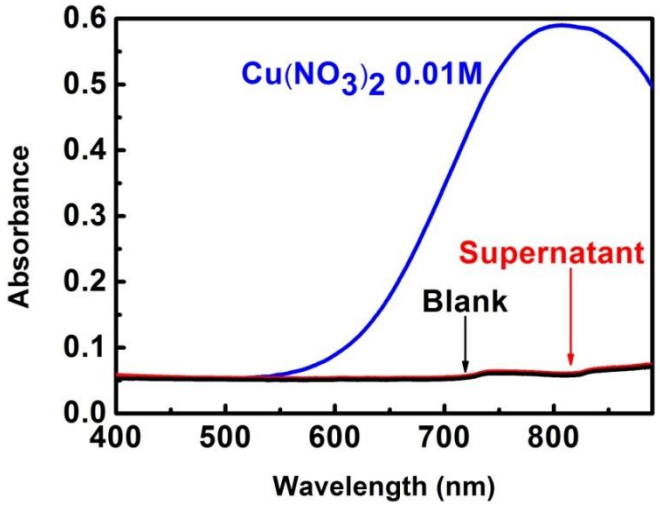

Fig. S1 The absorption spectrum collected on the colorless supernatant (red curve) after a full decantation by gravity of particles of $Cu_{0.9}Mg_{0.1}(OH)_2$ (x=0.1) taking place during the ageing period of 15h.

S1.2 X-Ray Powder Diffraction (XRPD)

The phase purity of as-prepared powders was checked by recording X-ray powder diffraction (XRPD) patterns at room temperature on a PANalytical θ/θ Bragg-Brentano Empyrean diffractometer ($CuK\alpha_{1+2}$ radiations) equipped with the PIXcel^{1D} detector. The raw powders were dusted through a 160 μm sieve on a glass holder at ambient air atmosphere (RH 60 %). XRPD patterns were collected at room temperature in the [5°-135°] scattering angle range, with a 0.0131° step size, for a total acquisition time of 330 min.

Thermal decomposition in air of as-prepared powders was studied by temperature-controlled X-ray powder diffraction. Temperature-controlled XRPD patterns were recorded on the same diffractometer at 25 °C intervals between 25 and 400 °C (heating rate of 10 °C.min^{-1}, temperature stabilisation for 20 min, cooling rate of 60°C.min^{-1}, air flow of 40 mL.min^{-1}) by using an XRK 900 Anton Paar reactor chamber. The sample was deposited on the sieve (pore size ∅ 0.2mm) of the open sample holder cup, both made of glass ceramic Macor ® , thus allowing gas to flow through the sample. Each XRPD pattern was collected at each temperature in the [10°-100°] scattering angle range, with a 0.0131° step size, for a total acquisition time of 180 min.

The average apparent size $<S_\beta>$ and the average lattice strain $<\varepsilon_\beta>$ of nanometer-sized particles were determined from diffraction data by the Integral Breadth method [1-4]. The patterns of the reference material $Na_2Ca_3Al_2F_{14}$ (NAC [5]) and the studied samples were refined by the Le Bail method [6] with the Fullprof program [7] using a modified Thompson-Cox-Hastings pseudo-Voigt profile function [8] (referred to as TCH-Z function) in which the size-broadening and microstrain-broadening effects both contribute to the Lorentzian and Gaussian components of the line widths. The "Needle vector size" model of the Fullprof program [7] was selected with the [0k0] direction parallel to the revolution axis of the needle. In a simplified approach, the size-broadening effect was assumed to only contribute to the Lorentzian component (one adjustable parameter) of the line widths while the Gaussian component (one adjustable parameter) would only arise from the microstrain. The average apparent size $<S_\beta>$ and the average lattice strain $<\varepsilon_\beta>$, were then calculated from those two components, respectively [9].

S1.3 Infrared (IR) spectroscopy

IR transmission spectra were collected on as-prepared polycrystalline samples in air at room temperature with an Alpha Bruker Fourier transform infrared (FT-IR) spectrometer equipped with the "Platinum" QuickSnap™ ATR sampling module. Each spectrum was obtained after 25 scans in the 4000-400 cm^{-1} range with a spectral resolution of 4 cm^{-1}. A reference IR spectrum was collected in the same conditions without any sample and subtracted to spectra collected on specimens in order to remove the contribution of atmospheric water vapor and carbon dioxide gas.

S1.4 Thermal analyses

The thermal decomposition of as-prepared powders was studied by thermogravimetric (TG) and Mass Spectrometric (MS) evolved gas analyses. Desorption of water molecules adsorbed on the particle surface was carried out in static air at 60 °C prior to any analysis. Thermal analyses were then performed from room temperature to 800 °C on a Jupiter NETZSCH STA449 F3 thermogravimetric analyser by heating at 2°C.min^{-1} about 50 mg of degassed sample in open alumina crucible under a controlled argon flow of 60 mL.min^{-1}. Three cycles of vacuum purging were performed before starting the experiment in order to remove any trace of atmospheric gases (N_2, O_2, CO_2 and of water vapor) present in the thermobalance. The gases evolved in the thermal analyses were monitored with a Aeolos Quadrupole Mass Spectrometer 403C coupled to the thermal balance via a stainless steel capillary heated to 250 °C. The mass gates used were m/z 17 (OH), 18 (H_2O), 28 (CO), 30 (NO), 44 (CO_2) and 46 (NO_2).

S1.5 Transmission Electron Microscopy (TEM)

The TEM study was performed on a JEOL JEM 2100 HR electron microscope operating at 200 kV and equipped with a side entry ± 35° double-tilt specimen holder. The sample for transmission electron microscopy investigation was prepared by ultrasonically dispersing the raw powder in absolute ethanol, depositing a drop of the resulting suspension onto a holey carbon-coated copper grid (or nickel grid for EDX analyses) and finally drying the grid in air. Chemical analysis was done on a large number of individual particles with an Energy-Dispersive X-ray (EDX) spectrometer JEOL JED-2300 T attached to the microscope.

S1.6 Nitrogen sorption measurements

N_2 adsorption measurements were performed at -196 °C on a Micromeritics TriStar II 3020 Instrument (Micromeretics, Norcross, GA). Prior to any surface area measurement, water vapour and gases adsorbed onto the grain surface were desorbed under primary vacuum by using the Micromeritics VacPrep 061 degasser. Approximately 400 mg of powder was employed in each measurement. All samples exhibit a type II adsorption isotherm typical of nonporous solids. The specific surface area was calculated using the Brunauer − Emmet − Teller (BET) model [10].

S1.7 Microwave Plasma - Atomic Emission Spectroscopy (MP-AES)

Atomic Emission spectroscopy has been used for measuring the amount (down to 0.05 ppm) of magnesium and copper elements possibly released from mixed hydroxides $Cu_{1-x}Mg_{1-x}(OH)_2$ when immersed in deionized water. Particles are immersed in deionized water at a final concentration of 1 $mg.mL^{-1}$ without agitation for 180 min or 1440 min. Concentration in magnesium and copper ions released by hydroxides particles was determined by using a 4100 Micro Plasma - Atomic Emission Spectrometer (MP-AES) from Agilent Technologies. The apparatus is equipped with a OneNeb nebulizer and a double-pass cyclonic spray chamber. The analytical cycle consisted of 15 s of sample uptake (pump speed 40 rpm) then 15 s of stabilization before performing three replicates. Calibration solutions were prepared by dilution of the ICP multi-element standard VIII solution (100 $mg.L^{-1}$, Merck) in the range 0.05-10 $mg.L^{-1}$. 5 mL of supernatant solution were manually introduced by using a capillary. When concentration in cations was above the calibration range, a dilution was then carried out. Integration time was set to 3 s both for magnesium and copper ions. Background was automatically subtracted from the signals by activating the blank subtraction mode of the MP Expert software from Agilent Technologies. The peak intensity was also determined by this software. Calibrations functions for the MP-AES measurements were linear up to 10 $mg.mL^{-1}$ for copper ions ($r^2 > 0.999$, 324.754 nm) and 5 $mg.mL^{-1}$ for magnesium ions ($r^2 > 0.995$, 285.213 nm).

S1.8 pH measurement of particle suspension

Particles are immersed in deionized water at a final concentration of 1 mg.mL^{-1} without agitation. At regular intervals between 15 min and 1440 min, pH of the aged solution was then measured at room temperature with a SCHOTT GERÄTE CG818 pH-meter.

S2. Thermal decomposition of $Cu_{1-x}Mg_x(OH)_2$ samples monitored by ThermoGravimetric (TG)-Mass Spectrometric (MS) evolved gas analyses

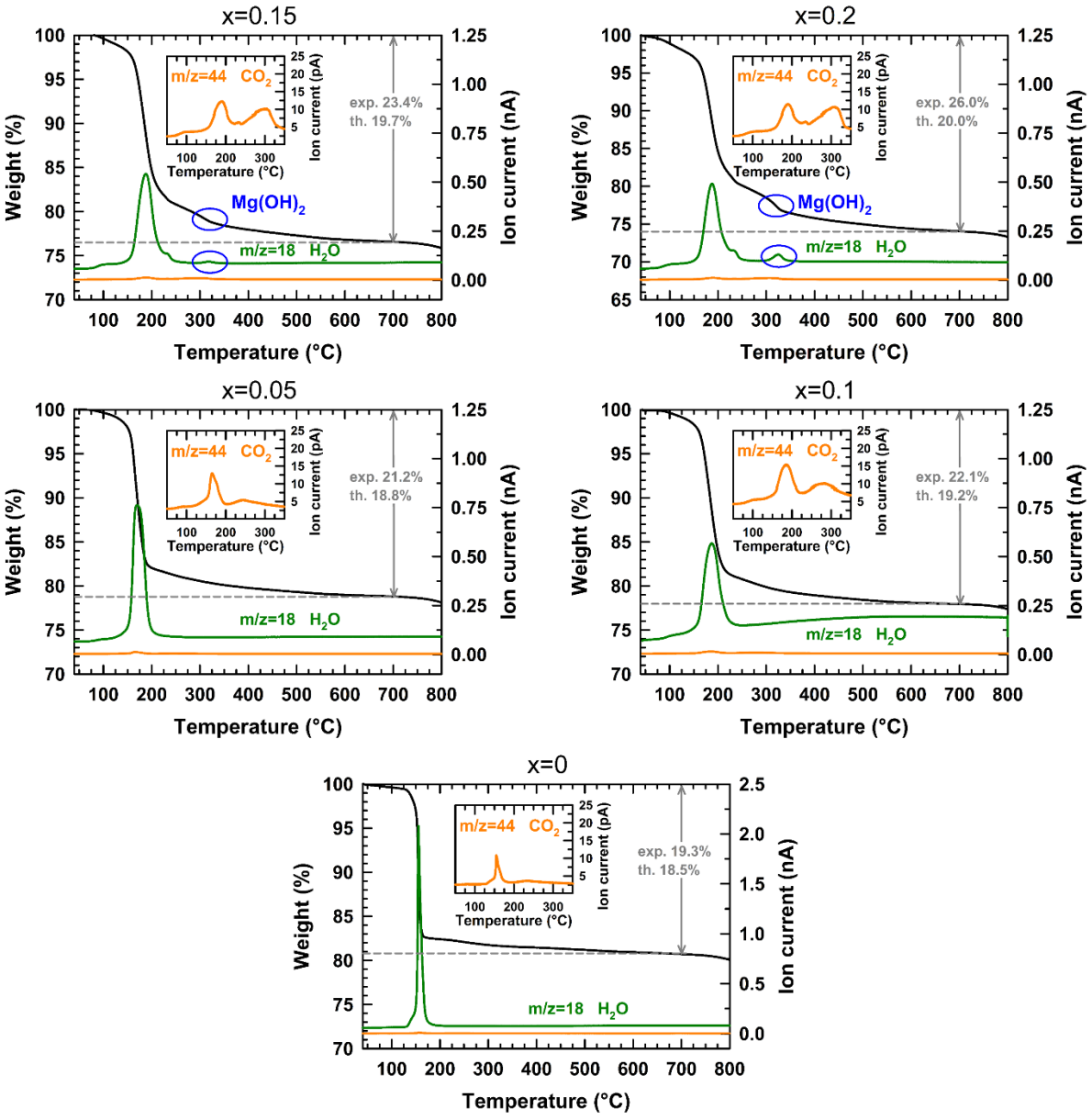

Fig. S2 TGA thermograms and Mass Spectra of released water and carbon dioxide collected upon heating in argon on $Cu(OH)_2$ (x = 0), $Cu_{0.95}Mg_{0.05}(OH)_2$ (x = 0.05), $Cu_{0.9}Mg_{0.1}(OH)_2$ (x = 0.10), $Cu_{0.85}Mg_{0.15}(OH)_2$ (x = 0.15) and $Cu_{0.8}Mg_{0.2}(OH)_2$ (x = 0.20) raw powder samples.

S3. Crystallographic data of $Cu_{1-x}Mg_x(OH)_2$ samples

Table S1 Results of Le Bail refinement for $Cu_{1-x}Mg_x(OH)_2$ nanorods (orthorhombic space group C $mc2_1$ (No.36)) from X-Ray Powder Diffraction (XRPD) Data. For each magnesium content x, the orthorhombic cell parameter *a*, *b* and *c* are listed as well as R-factors values for the fit.

Magnesium content x	a (Å)	b (Å)	c (Å)	R_p (%)	R_{wp} (%)	R_{exp} (%)
0	2.9507(2)	10.597(1)	5.2632(5)	8.16	7.14	2.95
0.05	2.9585(2)	10.6023(9)	5.2534(4)	7.51	6.64	3.29
0.10	2.9641(2)	10.615(1)	5.2350(4)	7.61	7.03	3.73
0.15	2.9675(2)	10.622(2)	5.2375(5)	9.22	8.47	3.41
0.20	2.9709(2)	10.622(2)	5.2341(5)	8.51	8.06	3.33

S4. Bactericidal activity of bi-phasic $Cu_{0.85}Mg_{0.15}(OH)_2$ and $Cu_{0.80}Mg_{0.20}(OH)_2$ samples

Table S2 Bactericidal activity of bi-phasic $Cu_{0.85}Mg_{0.15}(OH)_2$ and $Cu_{0.80}Mg_{0.20}(OH)_2$ nanorods (1 $mg.mL^{-1}$) against *E. coli* CIP 53126 and *S. aureus* CIP 4.83 (average value±standard deviation over 2 assays).

Magnesium content x	Contact time (min)	*E. coli*			*S. aureus*		
		$Log_{10}N_0$	$Log_{10}(N_0/N_t)$	Reduction (%)	$Log_{10}N_0$	$Log_{10}(N_0/N_t)$	Reduction (%)
0.15 (biphasic, 2nd phase =$Mg(OH)_2$)	15	6.72±0.02	0.43±0.13	61.1±11.1	6.63±0.11	0.85±0.02	85.8±0.6
	30		0.80±0.18	82.7±6.7		0.93±0.05	88.2±1.2
	60		2.25±0.30	99.3±0.4		1.23±0.06	94.0±0.9
	180		6.72±0.02	100		1.94±0.32	98.5±0.9
0.20 (biphasic, 2nd phase =$Mg(OH)_2$)	15	6.72±0.02	0.44±0.04	63.3±3.3	6.63±0.11	0.85±0.02	85.8±0.6
	30		0.93±0.03	88.1±0.7		1.02±0.05	90.4±1.1
	60		3.11±1.22	99.4±0.7		1.27±0.07	94.5±0.9
	180		6.72±0.02	100		1.85±0.18	98.5±0.6

S5. EPR spectra of the aerated water suspensions of $Cu(OH)_2$ and $Cu_{0.90}Mg_{0.10}(OH)_2$ nanorods in the presence of DMPO spin trapping agent

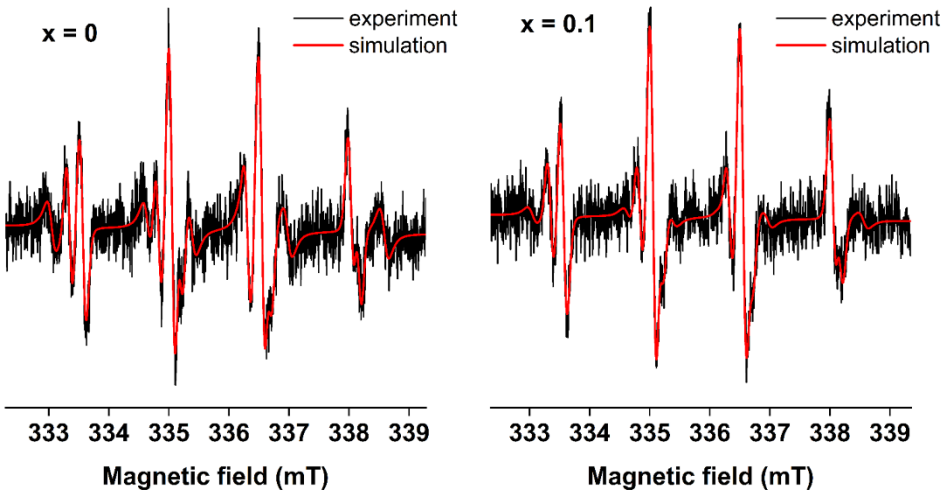

Fig. S3 Normalized experimental (black line) and simulated (red line) EPR spectra measured 22 min after the addition of DMPO spin trapping agent (c_0(DMPO) = 0.04 M) to the aerated water suspensions of $Cu(OH)_2$ (x = 0) and $Cu_{0.9}Mg_{0.1}(OH)_2$ (x = 0.1) nanorods (loading 1 $mg.mL^{-1}$).

S6. References

1. J. I. Langford, *J. Appl. Crystallogr.*, 1978, **11**, 10-14.
2. T. H. de Keijser, J. I. Langford, E. J. Mittemeijer and A. B. P. Vogels, *J. Appl. Crystallogr.*, 1982, **15**, 308-314.
3. J. I. Langford, D. Louër, E. J. Sonneveld and J. W. Visser, *Powder Diffraction*, 1986, **1**, 211-221.
4. J. I. Langford, *International Conference "Accuracy in Powder Diffraction II", May 26-29, 1992 at NIST, Gaithersburg, MD, USA*, 1992, 110-126.
5. G. Courbion and G. Ferey, *Journal of Solid State Chemistry*, 1988, **76**, 426-431.
6. A. Le Bail, H. Duroy and J. L. Fourquet, *Materials Research Bulletin*, 1988, **23**, 447-452.
7. J. Rodriguez Carvajal, *Physica B*, 1993, **192**, 55-69.
8. P. Thompson, D. E. Cox and J. B. Hastings, *J. Appl. Crystallogr.*, 1987, **20**, 79-83.
9. R. Delhez, T. H. de Keijser and E. J. Mittemeijer, *Fresenius' Zeitschrift für analytische Chemie*, 1982, **312**, 1-16.
10. S. Brunauer, P. H. Emmett and E. Teller, *Journal of the American Chemical Society*, 1938, **60**, 309-319.